Inorganic Chemistry

Article

pubs.acs.org/IC

New Hybrid Layered Molybdates Based on $^2/_\infty[Mo_nO_{3n+1}]^{2-}$ Units (n = 7, 9) with Systematic Organic–Inorganic Interfaces

Martine Bujoli-Doeuff, Rémi Dessapt,* Philippe Deniard, and Stéphane Jobic

Institut des Matériaux Jean Rouxel, Université de Nantes, CNRS, 2 rue de la Houssinière, BP 32229, 44322 Nantes Cedex 3, France

Supporting Information

ABSTRACT: Two new hybrid organic–inorganic molybdates based on layered $^2/_\infty[Mo_nO_{3n+1}]^{2-}$ blocks and organoammonium cations $^+(Me_xH_{3-x}N)$-$(CH_2)_6(NH_{3-x}Me_x)^+$ (x = 0–1), namely, $(H_3N(CH_2)_6NH_3)[Mo_7O_{22}]\cdot H_2O$ (**1**) and $(MeH_2N(CH_2)_6NH_2Me)[Mo_9O_{28}]$ (**2**), have been synthesized under hydrothermal conditions. The $^2/_\infty[Mo_9O_{28}]^{2-}$ unit in **2** is an unprecedented member of the $^2/_\infty[Mo_nO_{3n+1}]^{2-}$ family with the n value extended to 9. The structural filiation between the $^2/_\infty[Mo_nO_{3n+1}]^{2-}$ (n = 5, 7, 9) blocks is well established, and their structural similarity with the $^2/_\infty[MoO_3]$ slabs in α-MoO_3 is also discussed. Single-crystal X-ray analyses show that the $^2/_\infty[Mo_nO_{3n+1}]^{2-}$ layers in **1** and **2** are pillared in the three-dimensional networks by the organic cations with a similar connection at the organic–inorganic interface. In addition, a correlation between the topology of the $^2/_\infty[Mo_nO_{3n+1}]^{2-}$ blocks in **1** and **2** and the overall sizes of the associated organic cations is pointed out. Finally, the efficiency of Fourier transform Raman spectroscopy to easily discriminate the different $^2/_\infty[Mo_nO_{3n+1}]^{2-}$ blocks (n = 5, 7, 9) in hybrid organic–inorganic layered molybdate materials is clearly evidenced.

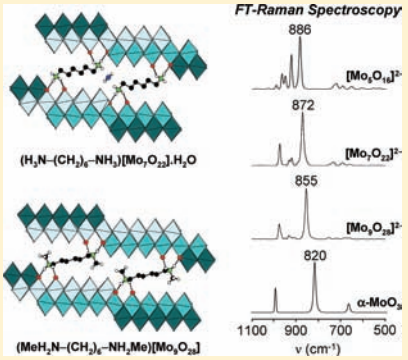

1. INTRODUCTION

Hybrid organic–inorganic assemblies of polyoxometalate (POM) building blocks and organic molecules[1] are of great interest for their potential applications in a wide range of fields including catalysis,[2] medicine,[3] photocatalysis,[4] and nanotechnology.[5] Such materials constitute a good opportunity to combine in a single phase the unique properties of the organic and inorganic moieties,[6] and because these properties often depend on the connection of both components, one of the main challenges for any hybrid materials designer indubitably remains the tailoring of the self-assembling processes.[7] To address this challenge is all the more important because new properties can also arise as a result of a synergetic effect at the interface itself.[8] In that context, photochromic hybrid materials based on POMs and organoammonium cations (OACs) are quite representative systems.[9] The photoresponses of such supramolecular crystallized networks drastically depend on the potential establishment of direct hydrogen-bonding interactions at the organic–inorganic interface. Hence, control of the positioning of the OACs toward the POMs should be of a great interest to monitor their optical properties.

Anticipating the hydrogen-bonding network of such materials needs to predict the number of hydrogen bonds, as well as the nature of the implied O atoms of the POM units. Unfortunately, it remains a difficult task to achieve, especially in cases of hybrid materials containing isolated zero-dimensional (0D-)POM clusters[10] or one-dimensional (1D-)POM chains.[11] This stems essentially from the great degree of freedom of the OACs in connecting the POMs. In our quest of rationalization, we have suspected that the assembly of OACs with layered molybdates $[Mo_xO_y]^{z-}$, which can be viewed as two-dimensional (2D-)POM building blocks, should allow better control of the organic–inorganic interface, considering that, at first sight, the higher the dimensionality of the mineral framework, the more restricted the interacting schemes between organic and inorganic components. On the basis of this crude assumption, we recently reported an efficient method to easily synthesize the rare molybdates $^2/_\infty[Mo_nO_{3n+1}]^{2-}$ (where n is odd and n = 5, 7), using $Na_2MoO_4\cdot 2H_2O$ as the molybdenum source and organoammonium dications (hereafter labeled A^{2+} cations) with the general formula $^+(Me_{3-x}H_xN)$-$(CH_2)_2(NH_yMe_{3-y})^+$ (x, y = 1–3).[12] Because in these systems the A^{2+} cations act as structure-directing agents for molybdate condensation, we suspected that the topology of the layered molybdates should be strongly correlated to the nature of the associated A^{2+} cations, and hence $^2/_\infty[Mo_nO_{3n+1}]^{2-}$ blocks with the upper n value should be accessible by using A^{2+} cations with larger sizes. With this aim, we have investigated the reactivity of MoO_4^{2-} toward $^+H_3N(CH_2)_6NH_3^+$ and $^+MeH_2N$-$(CH_2)_6NH_2Me^+$ cations. In the present work, we report the synthesis of two new hybrid materials, $(H_3N(CH_2)_6NH_3)$-$[Mo_7O_{22}]\cdot H_2O$ (**1**) and $(MeH_2N(CH_2)_6NH_2Me)[Mo_9O_{28}]$ (**2**). While **1** is built on the known $^2/_\infty[Mo_7O_{22}]^{2-}$ layer, **2** contains an unprecedented layered molybdate block, i.e., the $^2/_\infty[Mo_9O_{28}]^{2-}$ unit, which turns out to be a new member of the $^2/_\infty[Mo_nO_{3n+1}]^{2-}$ family with the n value extended to 9. The present work is organized as follows. Section 2 describes

Received: June 17, 2011
Published: December 15, 2011

   dx.doi.org/10.1021/ic201298d | Inorg. Chem. 2012, 51, 142–149

the experimental procedures followed to synthesize **1** and **2** as well as the physical techniques used to characterize them. Two detailed structural descriptions of the $^2/_\infty[Mo_5O_{16}]^{2-}$, $^2/_\infty[Mo_7O_{22}]^{2-}$, and $^2/_\infty[Mo_9O_{28}]^{2-}$ layers are provided in section 3 to point out their structural filiations. The structural similarity between the $^2/_\infty[Mo_nO_{3n+1}]^{2-}$ blocks and the $^2/_\infty[MoO_3]$ slabs in α-MoO_3 is also evidenced. A description of the supramolecular arrangement of the organic−inorganic interfaces in both **1** and **2** is then given. In addition, the use of Fourier transform (FT)-Raman spectroscopy as a powerful method to perfectly discriminate the different $^2/_\infty[Mo_nO_{3n+1}]^{2-}$ blocks is highlighted. Finally, the essential finding of this work is summarized in section 4.

2. EXPERIMENTAL SECTION

2.1. Synthesis. *Chemicals.* 1,6-Diaminohexane $N_2C_6H_{16}$ (HexDA), 1,6-bis(methylamino)hexane $N_2C_8H_{20}$ (DMHexDA), and $Na_2MoO_4{\cdot}2H_2O$ were purchased from Aldrich. All reagents were used without further purification.

$(H_3N(CH_2)_6NH_3)[Mo_7O_{22}]{\cdot}H_2O$ (1). $Na_2MoO_4{\cdot}2H_2O$ (0.242 g, 1 mmol) was dissolved in 20 mL of water. After the addition of HexDA (0.232 g, 2 mmol), the pH was adjusted with 4 M HCl to 1. The mixture was then stirred at room temperature for a few minutes and sealed in a 30 mL Teflon-lined autoclave (130 °C, 48 h, autogenous pressure). The resulting colorless blocks of **1** were filtered off, washed with H_2O and EtOH, and dried in air at room temperature. Yield in Mo: 47%. Anal. Calcd for $C_6H_{20}O_{23}N_2Mo_7$: C, 6.21; H, 1.72; N, 2.41; Mo, 57.93. Found: C, 6.23; H, 1.71; N, 2.38; Mo, 57.33. FT-IR (cm^{-1}): ν(Mo═O, Mo−O−Mo) 922 (s), 901 (s), 874 (s), 841 (vs), 737 (w), 696 (w), 644 (m), 546 (m), 519 (m), 467 (m), 445 (w). From differential scanning calorimetry/thermogravimetric analysis (DSC/TGA) measurements, **1** loses the water molecules above 170 °C and decomposes beyond 290 °C.

$(MeH_2N(CH_2)_6NH_2Me)[Mo_9O_{28}]$ (2). $Na_2MoO_4{\cdot}2H_2O$ (0.242 g, 1 mmol) was dissolved in 20 mL of water. After the addition of DMHexDA (0.288 g, 2 mmol), the pH was adjusted with 4 M HCl to 1. The mixture was then stirred at room temperature for a few minutes and sealed in a 30 mL Teflon-lined autoclave (130 °C, 48 h, autogenous pressure). The resulting colorless blocks of **2** were filtered off, washed with H_2O and EtOH, and dried in air at room temperature. Yield in Mo: 86%. Anal. Calcd for $C_8H_{22}O_{28}N_2Mo_9$: C, 6.58; H, 1.51; N, 1.92; Mo, 59.26. Found: C, 6.74; H, 1.55; N, 1.91; Mo, 58. FT-IR (cm^{-1}): ν(Mo═O, Mo−O−Mo) 931 (s), 899 (vs), 831 (s), 737 (s), 696 (s), 634 (m), 577 (m), 528 (m), 476 (m), 445 (w). From DSC/TGA measurements, **2** decomposes beyond 310 °C.

2.2. Structure Determination. Solvent-free glue was used to firmly fix the crystals of **1** and **2** at the tip of Lindemann capillaries. Data collections were carried out at 120 K for crystal **1** and at room temperature for crystal **2** on a Bruker-Nonius Kappa CCD diffractometer using Mo K-$L_{2,3}$ radiation with a graphite monochromator. Intensity integration and standard Lorentz-polarization corrections were done with the *JANA2006* program suite,[13] using the crystal shape for absorption correction (Gaussian method). Structure determination was done with the charge-flipping method[14,15] with Superflip,[16] a built-in part of *JANA2006*. Obtained structures were visualized and plotted with the *Diamond* program.[17] Starting from the obtained model, all Mo and O atoms could be located. The C atoms were subsequently found through difference Fourier synthesis. Using anisotropic atomic displacement parameters, adding H atoms at calculated positions with angle and distance restraints allowed one to make the refinement smoothly converge. Residual factors are given in Table 1 for the two structures. CCDC 826645 (**1**) and 826646 (**2**) contain the supplementary crystallographic data for this paper. These data can be obtained free of charge via www.ccdc.cam.ac.uk/conts/retrieving.html (or from the Cambridge Crystallographic Data Centre, 12 Union Road, Cambridge CB21EZ, U.K.; fax (44) 1223-336-033; e-mail deposit@ccdc.cam.ac.uk).

Table 1. Crystallographic Data for 1 and 2

	1	2
(a) Physical, Crystallographic, and Analytical Data		
empirical formula	$Mo_7O_{23}C_6H_{20}N_2$	$Mo_9O_{28}C_8H_{22}N_2$
M_r (g mol^{-1})	1159.8	1457.7
cryst syst, space group	monoclinic, $P2/c$	monoclinic, $C2/c$
a (Å)	11.623 (3)	23.6437 (13)
b (Å)	5.4942 (4)	5.4528 (8)
c (Å)	19.495 (6)	24.7496 (14)
β (deg)	103.10 (4)	109.699 (2)
V (Å^3)	1212.5 (6)	3004.1 (5)
Z	2	4
F_{000}	1096	2744
D_x (g cm^{-3})	3.170	3.222
radiation λ (Å)	Mo K-$L_{2,3}$	Mo K-$L_{2,3}$
	0.710 69	0.710 69
μ (mm^{-1})	3.61	3.74
T (K)	120	293
cryst shape, size	plate, colorless	block, colorless
cryst dimens (mm)	0.06 × 0.03 × 0.02	0.10 × 0.09 × 0.07
(b) Data Collection and Data Reduction		
diffractometer	Nonius CCD	Nonius CCD
radiation source	Mo K-$L_{2,3}$	Mo K-$L_{2,3}$
monochromator	graphite	graphite
scan mode	ϕ, ω scans	ϕ, ω scans
abs corrn	Gaussian *JANA2006* (Petricek et al., 2000)	Gaussian *JANA2006* (Petricek et al., 2000)
transmn	T_{min} = 0.579, T_{max} = 0.782	T_{min} = 0.579, T_{max} = 0.782
measd reflns	56 062	21 462
indep reflns	5306	6486
reflns with $I > 2\sigma(I)$	3177	3284
R_{int}	0.122	0.134
θ_{max} (deg)	35	35
θ_{min} (deg)	6.4	6.6
	h = −18 → 18	h = −38 → 35
	k = −8 → 8	k = −7 → 8
	l = −31 → 31	l = −39 → 39
(c) Refinement		
refinement	F^2	F^2
$R[F^2 > 2\sigma(F^2)]$	0.040	0.057
$R_w(F^2)$	0.078	0.103
S	1.10	1.20
no. of reflns	3177	3284
no. of param	176	214
no. of constraints	38	44
weighting scheme	$w = 1/[\sigma^2(I) + 0.001936I^2]$	$w = 1/[\sigma^2(I) + 0.001936I^2]$
$\Delta\rho_{max}$ (e Å^{-3})	1.51	2.03
$\Delta\rho_{min}$ (e Å^{-3})	−1.57	−2.00
extinction correction	none	B−C type 1 Lorentzian isotropic (Becker and Coppens, 1974)

2.3. Physical Measurements. Elemental analyses of the solids were performed by the "Service d'Analyse du CNRS" in Vernaison, France. FT-IR spectra were recorded in the 4000−400 cm^{-1} range on a Bruker Vertex equipped with a computer control using *OPUS* software. FT-Raman spectra were collected at room temperature under an excitation wavelength of 1064 nm (Nd:YAG laser) using a FT-Raman Bruker RFS 100 spectrophotometer. The nominal power was modulated between 100 and 340 mW to avoid any degradation of the

dx.doi.org/10.1021/ic201298d | *Inorg. Chem.* 2012, 51, 142−149

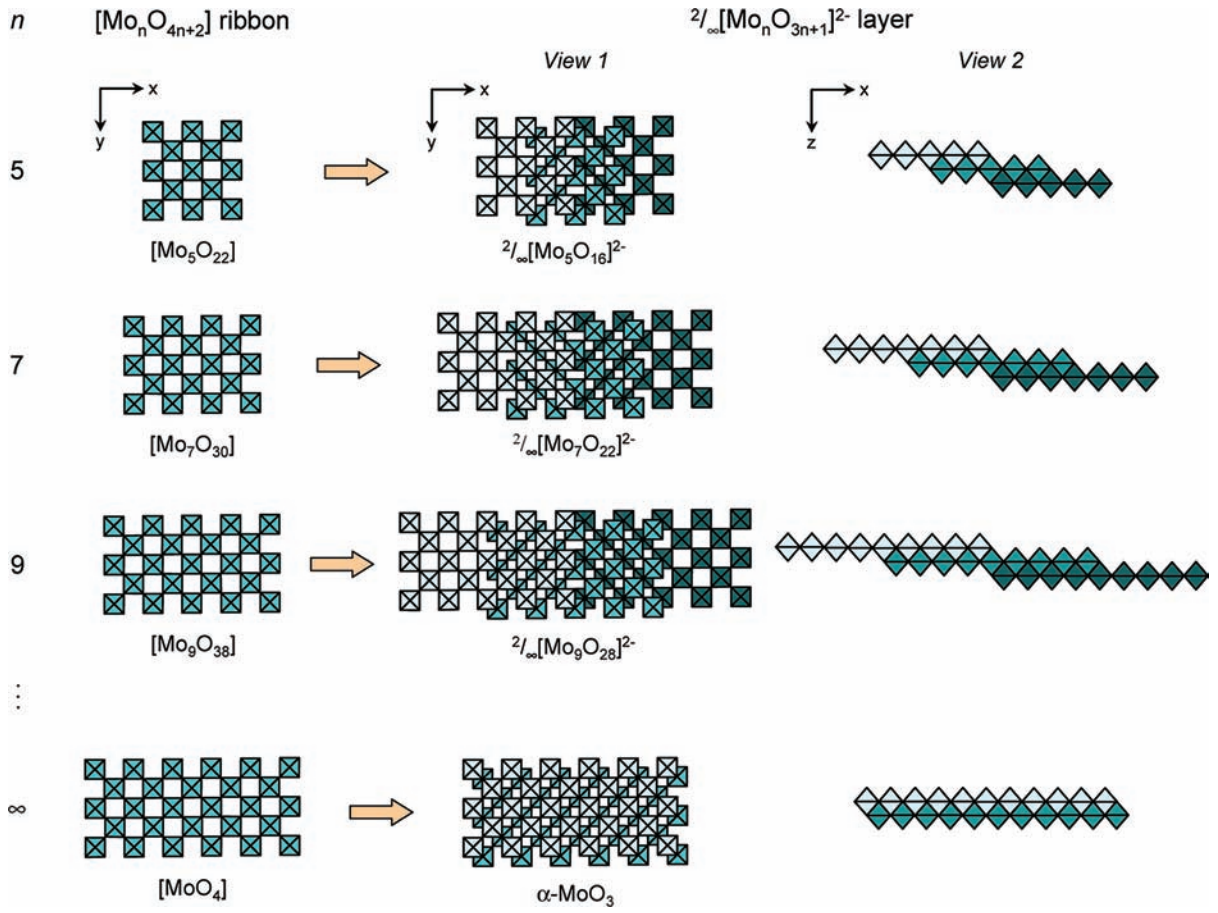

Figure 1. Schematic idealized representations of the $^{2}/_{\infty}[Mo_nO_{3n+1}]^{2-}$ layers (n = 5, 7, and 9) and α-MoO_3 built upon the stacking of $[Mo_nO_{4n+2}]$ ribbons (n = 5, 7, 9, and ∞, respectively): (view 1) in the xy plane, i.e., parallel to the normal of the layers; (view 2) in the xz plane, i.e., perpendicular to the normal of the layers.

materials. Spectra were recorded at 4 cm^{-1} resolution over the wavenumber range 100−3500 cm^{-1}, with a 1000 scan accumulation. DSC/TGA were measured by flowing dry argon with a heating and cooling rate of 5 °C min^{-1} on a SETARAM TG-DSC 111 between 20 and 800 °C.

3. RESULTS AND DISCUSSION

3.1. Synthesis. **1** and **2** have been synthesized pure and in good yields, in a one-pot reaction, by acidifying at pH 1 a mother solution initially containing $Na_2MoO_4{\cdot}2H_2O$ and the appropriate OAC and after keeping the mixture under hydrothermal conditions at 130 °C for 48 h. While **2** is the very first supramolecular hybrid molybdate network built upon the $^{+}MeH_2N(CH_2)_6NH_2Me^{+}$ cation, two other $^{+}H_3N(CH_2)_6NH_3^{+}$ containing 1D-POMs have already been reported, namely, $(H_3N(CH_2)_6NH_3)[Mo_3O_{10}]$[18] and $(H_3N(CH_2)_6NH_3)_2[Mo_8O_{26}]$.[19] None of them was detected as a byproduct in the synthesis of **1**. This could be explained considering that, in the literature, these materials were isolated for pH values higher than that of **1**. Formally, as the acidity of the molybdate entities increases in the sequence $^{1}/_{\infty}[Mo_3O_{10}]^{2-}$ < $^{1}/_{\infty}[Mo_8O_{26}]^{4-}$ < $^{2}/_{\infty}[Mo_7O_{22}]^{2-}$,[12] the formation of these three blocks from the acidification of MoO_4^{2-} theoretically requires increasing quantities of proton (Supporting Information). So, at first sight, the unique stabilization of the $^{2}/_{\infty}[Mo_7O_{22}]^{2-}$ entity could be imput to the very low pH value used for the synthesis of **1**.

3.2. Overall Description of the $^{2}/_{\infty}[Mo_nO_{3n+1}]^{2-}$ Layers (n = 5, 7, 9). The single-crystal X-ray analyses of **1** and **2** (Table 1) reveal that **1** is built on $^{2}/_{\infty}[Mo_7O_{22}]^{2-}$ layers, $^{+}H_3N(CH_2)_6NH_3^{+}$ cations, and water molecules, while **2** contains the $^{2}/_{\infty}[Mo_9O_{28}]^{2-}$ units and $^{+}MeH_2N(CH_2)_6NH_2Me^{+}$ cations only. Until now, the n value of the known $^{2}/_{\infty}[Mo_nO_{3n+1}]^{2-}$ layers was limited to 5[18a,20] and 7,[21] and thus the $^{2}/_{\infty}[Mo_9O_{28}]^{2-}$ block is the very first member of this family with n equal to 9. In this section, we present two complementary descriptions (hereafter noted as A and B) of the overall topology of the $^{2}/_{\infty}[Mo_nO_{3n+1}]^{2-}$ layers (n = 5, 7, 9) as well as that of α-MoO_3, which present many structural similarities (see below). The A description is useful to comprehend the design of the organic−inorganic interfaces in **1** and **2** (see section 3.2), while the B description makes easier the correlation between topologies and Raman signatures of the $^{2}/_{\infty}[Mo_nO_{3n+1}]^{2-}$ blocks (see section 3.3).

Description A. As depicted in Figure 1, the overall topology of the $^{2}/_{\infty}[Mo_nO_{3n+1}]^{2-}$ layers (n = 5, 7, 9) can be schematically described from infinite $[Mo_nO_{4n+2}]$ ribbons built upon corner-sharing $[MoO_6]$ octahedra.[21a] The ribbons defined in a xy plane are one octahedron thick and n octahedra broad (along x) and develop along y. Each ribbon is sandwiched via edge-sharing condensation between two identical ribbons shifted along x in two opposite directions with half-overlapping (Figure 1, view 1). It results in stairlike layered structures in which the step widths are exactly half of

dx.doi.org/10.1021/ic201298d | Inorg. Chem. 2012, 51, 142−149

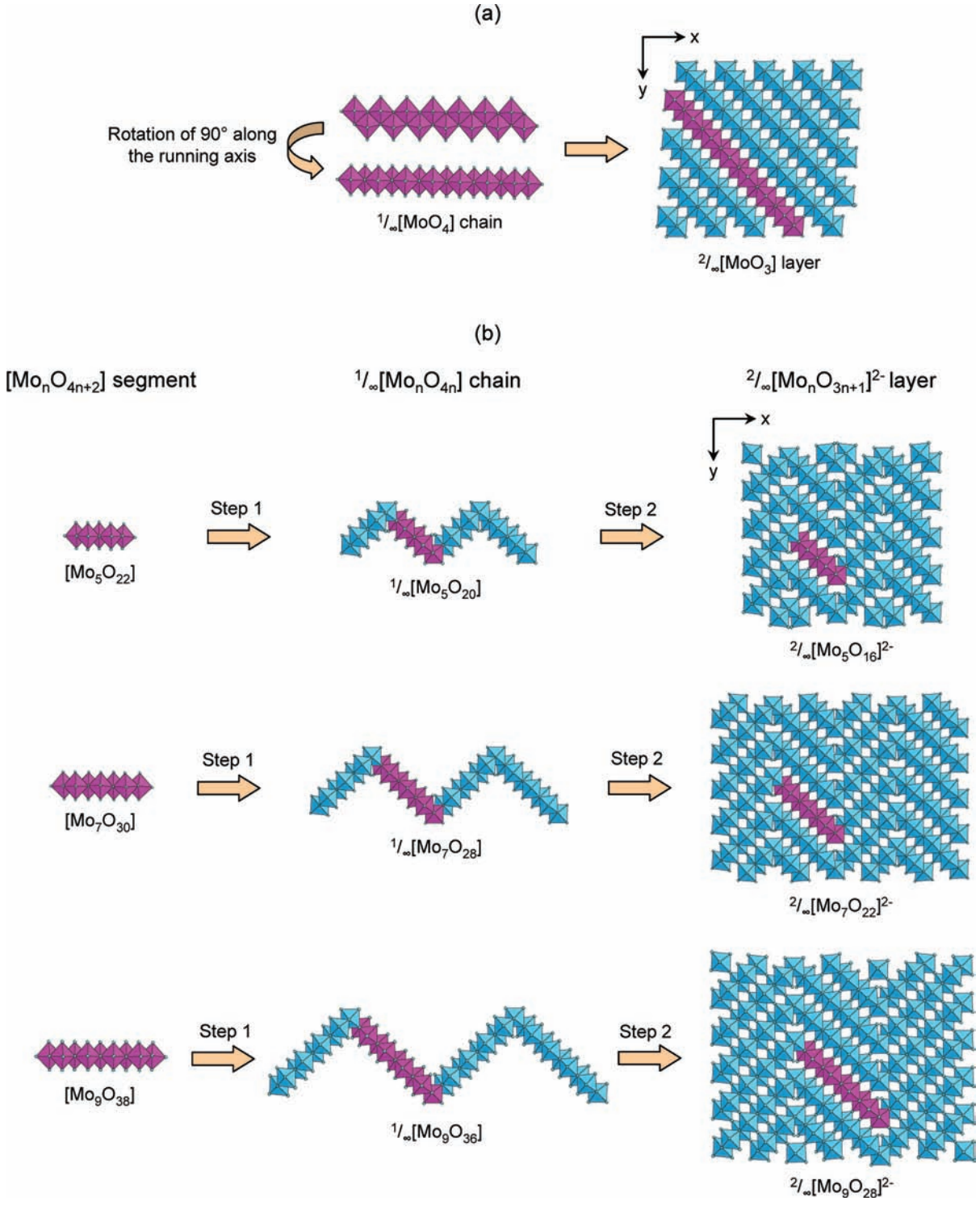

Figure 2. (a) Schematic building of the $^2/_\infty[MoO_3]$ layer in α-MoO_3 (displayed in the *xy* plane, i.e., parallel to the normal of the layers) from the linear $^1/_\infty[MoO_4]$ chain (in pink color) displayed along two directions perpendicular to the running axis. (b) Schematic building of the $^2/_\infty[Mo_nO_{3n+1}]$ layers (n = 5, 7, 9) (displayed in the *xy* plane, i.e., parallel to the normal of the layers) issued from a virtual two-step condensation mechanism of the linear $[Mo_nO_{4n+2}]$ segments (in pink color). Step 1: The segments condense via edge sharing in zigzag $^1/_\infty[Mo_nO_{4n}]$ chains. Step 2: The chains are connected via corner sharing to give rise to the $^2/_\infty[Mo_nO_{3n+1}]^{2-}$ layers.

those of the $[Mo_nO_{4n+2}]$ ribbons (Figure 1, view 2). Let us notice that the $^2/_\infty[Mo_nO_{3n+1}]^{2-}$ layers show strong structural similarities with the $^2/_\infty[MoO_3]$ slabs observed in the α form of molybdenum trioxide[22] (commonly called molybdite). Formally, α-MoO_3 consists of $^2/_\infty[MoO_4]$ sheets (Figure 1), which can be viewed as the ultimate member of the aforementioned $[Mo_nO_{4n+2}]$ ribbons when n tends to infinity. These $^2/_\infty[MoO_4]$ layered building blocks condense two at a time via edge-sharing to form $^2/_\infty[MoO_3]$ layers that are held together by van der Waals interactions. The main difference between the $^2/_\infty[Mo_nO_{3n+1}]^{2-}$ layers and molybdenum trioxide lies in the absence of steps in α-MoO_3.

dx.doi.org/10.1021/ic201298d | *Inorg. Chem.* 2012, 51, 142–149

Description B. An alternative description of the $^2/_\infty[Mo_nO_{3n+1}]^{2-}$ and α-MoO_3 layers is also depicted in Figure 2. Then, the molybdenum oxide layers of molybdite can be regarded as built upon linear $^1/_\infty[MoO_4]$ chains consisting of $[MoO_6]$ octahedra sharing cis-equatorial edges (Figure 2a). These chains are then connected via the sharing of apical corners to give rise to the $^2/_\infty[MoO_3]$ layers. Similarly, the $^2/_\infty[Mo_nO_{3n+1}]^{2-}$ blocks (n = 5, 7, 9) are constructed on linear $[Mo_nO_{4n+2}]$ segments of the $^1/_\infty[MoO_4]$ chains described above (Figure 2b). These segments condense via edge sharing to form zigzag $^1/_\infty[Mo_nO_{4n}]$ chains. These chains are then corner-shared-connected to give rise to the $^2/_\infty[Mo_nO_{3n+1}]^{2-}$ layers.

3.3. Description of the Organic–Inorganic Interfaces in 1 and 2. As shown in Figure 3, the $^2/_\infty[Mo_nO_{3n+1}]^{2-}$ layers

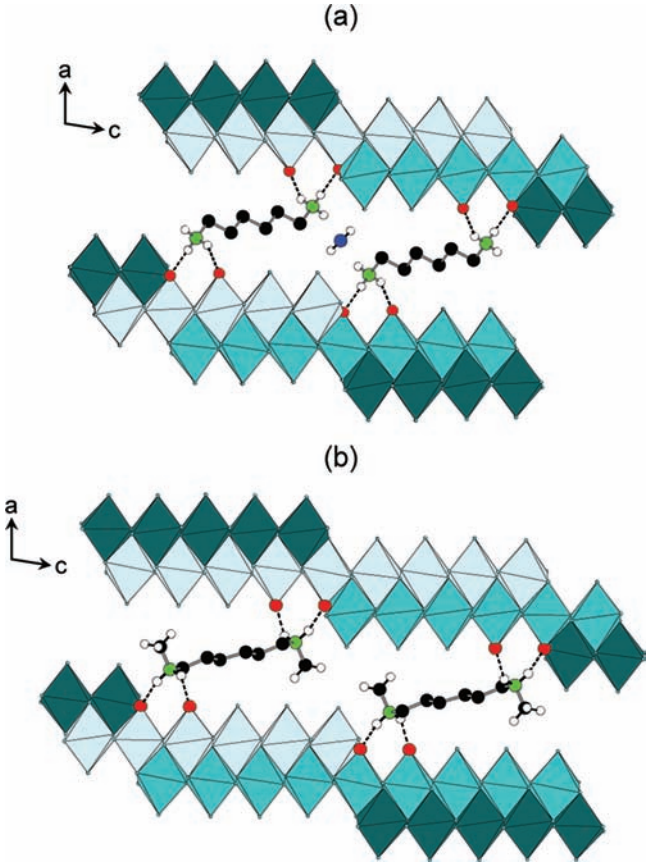

Figure 3. Representation of the organic–inorganic interfaces in (a) **1** and (b) **2**. Color code: H (white), C (black), N (green), μ^2-O and terminal O atoms of the $^2/_\infty[Mo_nO_{3n+1}]^{2-}$ layers implied in the hydrogen-bonding network (red), and O atoms of the water molecules (blue). The hydrogen-bonding networks between both the organic and inorganic components are displayed as dotted lines. For clarity, the H atoms of the CH_2 groups of the A^{2+} cations are omitted.

in **1** and **2** are stacked along the crystallographic *a* axis and they are pillared by the A^{2+} cations. The connection between both the organic and inorganic components is ensured by strong hydrogen-bonding interactions and follows the same interacting scheme. Namely, each ammonium head of the A^{2+} cations is anchored at the step of the $^2/_\infty[Mo_nO_{3n+1}]^{2-}$ layers and develops two N–H···O interactions, one with a terminal O atom of a given $[Mo_nO_{4n+2}]$ ribbon (O5 in **1** and O8 in **2**) and the other with a bridging μ^2-O that is common with the two vicinal ribbons constitutive of the $^2/_\infty[Mo_nO_{3n+1}]^{2-}$ layer (O9 and O7 in **1** and **2**, respectively; details related to the hydrogen bonds in **1** and **2** are given in Table 2). According to the bond

Table 2. Hydrogen-Bonding Geometry (Å and deg) in 1 and 2

X–H···O (X = N, O)	X–H	H···O	X···O	X–H···O
	Compound **1**			
N_1–H_{1N1}···O_w	0.92	1.97	2.864(5)	163.87
N_1–H_{3N1}···O_5	0.92	2.06	2.904(6)	152.04
N_1–H_{2N1}···O_9	0.92	1.92	2.833(5)	173.48
O_w–H_1···O_{11}	0.95	1.79	2.735(5)	169.63
	Compound **2**			
N_1–H_{1N1}···O_7	0.92	2.06	2.875(10)	147.43
N_1–H_{2N1}···O_8	0.92	2.16	2.965(13)	146.26

valence sum calculations, the terminal O atom is the second more nucleophilic site of each layered molybdate while the bridging O atom has a very weak nucleophilicity (Supporting Information, Tables S1 and S2). The complete hydrogen-bonding network in **1** also includes crystallized water molecules that develop two short hydrogen bonds (Table 2) with O11, which is the more nucleophilic oxide of the heptamolybdate blocks (Supporting Information, Table S1) and two longer N–H···O interactions with two adjacent $^+H_3N(CH_2)_6NH_3^+$ cations. At first sight, the hydrogen-bonding network in **1** matches well with the H-atom-donor and -acceptor strengths considering that, as is often observed in such hybrid materials, the short O–H···O interactions imply the water molecule that is the strong H-atom donor and the most nucleophilic oxide of the molybdates, while longer and weaker N–H···O interactions are established with less nucleophilic oxides. Let us notice that in the case of **2**, which contains no crystallized water molecules, the strongest nucleophilic oxide of the $^2/_\infty[Mo_9O_{28}]^{2-}$ block (O13) is not implied in any N–H···O interactions with the $^+MeH_2N(CH_2)_6NH_2Me^+$ cations. Hence, the anchoring of the ammonium heads at the steps of the molybdate layers would mainly originate from a steric hindrance factor than from the matching between H-atom-donor and -acceptor strengths (see below).

It is remarkable to notice that similar positions of the ammonium heads toward the steps of the $^2/_\infty[Mo_nO_{3n+1}]^{2-}$ layers with identical hydrogen-bonding networks are also observed in the reported $(A)[Mo_5O_{16}]$ materials, which gave rise to single-crystal X-ray investigations, i.e., $(MeH_2N(CH_2)_2NH_2Me)[Mo_5O_{16}]$,[12] $(H_3N(CH_2)_2NH_2Me)[Mo_5O_{16}]$,[12] $(H_3N(CH_2)_4NH_3)[Mo_5O_{16}]$,[18a] and $(H_2pipz)[Mo_5O_{16}]$[18b] (Supporting Information, Figure S1). To our knowledge, the $^2/_\infty[Mo_nO_{3n+1}]^{2-}$-containing hybrid materials appear as the unique OAC/POM family, which presents a systematic arrangement of the organic–inorganic interface.

Attempts to identify the chemical forces driving the formation of the $^2/_\infty[Mo_nO_{3n+1}]^{2-}$-containing hybrid materials are to date risky. However, as we expected, the topology of the molybdate layers depends on the nature of the associated A^{2+} cations, and $^2/_\infty[Mo_nO_{3n+1}]^{2-}$ blocks with n higher than 7 can be stabilized in the solid state by increasing the overall size of the organic component. This latter includes both the N···N interatomic distance and the size of the ammonium heads. At first sight, because both the $^+H_3N(CH_2)_6NH_3^+$ and $^+MeH_2N(CH_2)_6NH_2Me^+$ cations have similar N···N interatomic distances [8.750(6) and 8.788(13) Å, respectively], stabilization

dx.doi.org/10.1021/ic201298d | *Inorg. Chem.* 2012, 51, 142–149

of the $^2/_\infty[Mo_7O_{22}]^{2-}$ block in **1** and the $^2/_\infty[Mo_9O_{28}]^{2-}$ one in **2** should rather depend on the shape and steric hindrance of the ammonium heads. In **1**, the $^+H_3N(CH_2)_6NH_3^+$ cation has few blocked ($-NH_3^+$) groups and its overall size matches well with the step width of the $^2/_\infty[Mo_7O_{22}]^{2-}$ block. Two adjacent $^+H_3N(CH_2)_6NH_3^+$ cations are close to one another with a short intermolecular N···N distance of 4.900(7) Å. The interspace between the organic cations delimits small hydrophilic cavities, which contain the water molecules. At the opposite, the $^+MeH_2N(CH_2)_6NH_2Me^+$ cation has more blocked ($-NH_2Me^+$) heads and its overall size is quite a bit bigger (about 10.2 Å between the two methyl groups). Consequently, it cannot connect the $^2/_\infty[Mo_7O_{22}]^{2-}$ blocks similarly to the $^+H_3N(CH_2)_6NH_3^+$ cation because of strong steric repulsions between the methyl substituents of two adjacent cations. However, the overall size of the $^+MeH_2N(CH_2)_6NH_2Me^+$ cation is in better agreement with the step width of the $^2/_\infty[Mo_9O_{28}]^{2-}$ block in **2** (Figure 3b). In addition, the adjacent $^+MeH_2N(CH_2)_6NH_2Me^+$ cations are more distant [intermolecular N···N distance of 7.030(15) Å], which strongly reduces the steric repulsions between the methyl groups. Nevertheless, the latter reduces both the size and hydrophilicity of the aforementioned interlayer cavities, which should explain why no crystallized water molecules are intercalated in **2**.

3.4. Characterization of the $^2/_\infty[Mo_nO_{3n+1}]^{2-}$ Layer (n = 5, 7, 9) Blocks by FT-Raman Spectroscopy. The structural filiations between the $^2/_\infty[Mo_nO_{3n+1}]^{2-}$ layers (n = 5, 7, 9) and their similarities with the topology of the α-MoO_3 slabs can also be evidenced by FT-Raman spectroscopy. Figure 4 displays a comparison between the Raman spectra of **1**, **2**, $(MeH_2N(CH_2)_2NH_2Me)[Mo_5O_{16}]$,[12] and α-MoO_3 in the 1100−500 cm^{-1} range. The Raman signatures of the $^2/_\infty[Mo_nO_{3n+1}]^{2-}$ blocks (n = 5, 7, 9) are perfectly distinguishable by comparing the position in frequency of the strongest and sharp lines located at 886, 872, and 855 cm^{-1} for the $^2/_\infty[Mo_5O_{16}]^{2-}$, $^2/_\infty[Mo_7O_{22}]^{2-}$, and $^2/_\infty[Mo_9O_{28}]^{2-}$ units, respectively. This frequency shifts at 820 cm^{-1} for α-MoO_3 and is assigned by Seguin et al.[23] to the stretching mode of the Mo−O−Mo vibration (hereafter labeled as Mo_2O vibration). This specific vibration implies the O atoms that connect two $^1/_\infty[MoO_4]$ chains (Figure 2a). Thus, by analogy with α-MoO_3, the strong line observed in the Raman spectra of the $^2/_\infty[Mo_nO_{3n+1}]^{2-}$ blocks (n = 5, 7, 9) should be attributed to the Mo_2O vibration frequency (ν_{Mo_2O}), implying the corner-shared O atoms in common with two $[Mo_nO_{4n+2}]$ segments (Figure 2b). In experiments, ν_{Mo_2O} continuously decreases with increasing n, to reach its lower value for α-MoO_3. This should be qualitatively interpreted as follows. Let us consider x as the number of Mo_2O vibrators per Mo atom in the $^2/_\infty[Mo_nO_{3n+1}]^{2-}$ blocks and in α-MoO_3. On the basis of the structural analysis of the different layers depicted in Figure 2b, x is directly related to n according to eq 1 and equals 0.800, 0.857, 0.888, and 1.000 for $^2/_\infty[Mo_5O_{16}]^{2-}$, $^2/_\infty[Mo_7O_{22}]^{2-}$, $^2/_\infty[Mo_9O_{28}]^{2-}$, and α-MoO_3, respectively.

$$x = (n - 1)/n \quad (1)$$

Consequently, x increases with the length of the $[Mo_nO_{4n+2}]$ segments in the $^2/_\infty[Mo_nO_{3n+1}]^{2-}$ layers to reach its maximum value for the $^1/_\infty[MoO_4]$ chains of α-MoO_3. Thus, in the first approximation, it should signify that the average environment of the Mo centers in the $[Mo_nO_{4n+2}]$ segments progressively matches with that observed in the $^1/_\infty[MoO_4]$ chains of α-MoO_3. This should thus logically impact ν_{Mo_2O}. Figure 5 displays the ν_{Mo_2O} frequency as a function of x for **1**, **2**, and α-MoO_3 as well as seven other reported $^2/_\infty[Mo_5O_{16}]^{2-}$- and $^2/_\infty[Mo_7O_{22}]^{2-}$-containing hybrid materials (Supporting Information, Table S3). Surprisingly, ν_{Mo_2O} linearly decreases with x, according to the empirical relationship described in eq 2. This relationship has a predictive character, and it could be useful to easily identify new $^2/_\infty[Mo_nO_{3n+1}]^{2-}$ layers (especially with n higher than 9) in future powdered hybrid materials.

$$\nu_{Mo_2O}\ (cm^{-1}) = -322.7x + 1144.3 \quad (2)$$

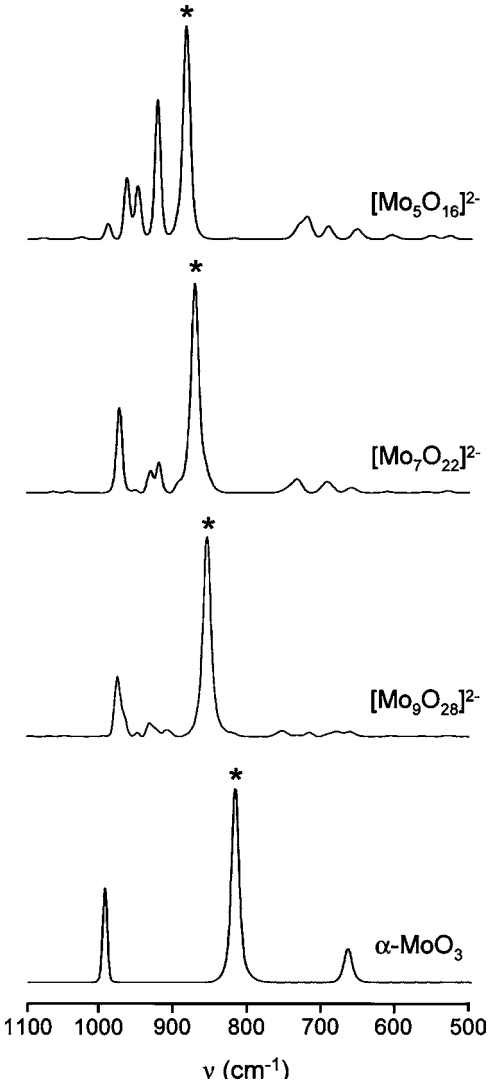

Figure 4. Comparison between the FT-Raman spectra of the $^2/_\infty[Mo_5O_{16}]^{2-}$ block in $(MeH_2N(CH_2)_2NH_2Me)[Mo_5O_{16}]$, the $^2/_\infty[Mo_7O_{22}]^{2-}$ block in **1**, the $^2/_\infty[Mo_9O_{28}]^{2-}$ block in **2**, and α-MoO_3. Asterisks denote the lines characteristic of the Mo_2O stretching vibration in the different molybdenum oxide layers.

4. CONCLUSION

We have synthesized two new hybrid organic−inorganic layered molybdate materials **1** and **2**. The $^2/_\infty[Mo_9O_{28}]^{2-}$ block in **2** is an unprecedented member of the $^2/_\infty[Mo_nO_{3n+1}]^{2-}$ family with n extended to 9. Our present work has highlighted that the assembly of the $^2/_\infty[Mo_nO_{3n+1}]^{2-}$

dx.doi.org/10.1021/ic201298d | Inorg. Chem. 2012, 51, 142−149

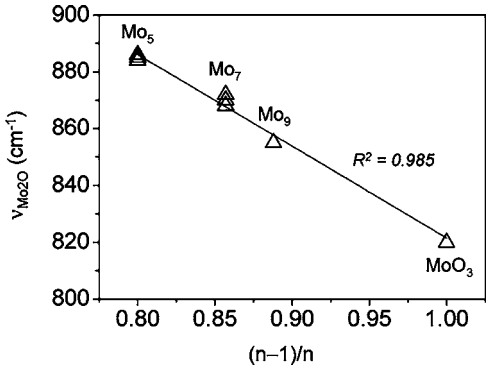

Figure 5. Mo_2O vibration frequency versus $x = (n - 1)/n$, i.e., the number of Mo_2O vibrators per Mo atom for the $^2/_\infty[Mo_5O_{16}]^{2-}$ block (Mo_5) in $(MeH_2N(CH_2)_2NH_2Me)[Mo_5O_{16}]$, $(H_3N(CH_2)_2NH_2Me)[Mo_5O_{16}]$, $(H_2pipz)[Mo_5O_{16}]$, $(H_3N(CH_2)_4NH_3)[Mo_5O_{16}]$, the $^2/_\infty[Mo_7O_{22}]^{2-}$ block (Mo_7) in **1**, $(MeNH_3)_2[Mo_7O_{22}]$, $(Me_2HN(CH_2)_2NH_2Me)[Mo_7O_{22}]$, and $(Me_2HN(CH_2)_2NHMe_2)[Mo_7O_{22}]$, and the $^2/_\infty[Mo_9O_{28}]^{2-}$ block (Mo_9) in **2** and α-MoO_3. R^2 is the regression coefficient of the linear fitting.

layers and the A^{2+} cations in **1** and **2** as well as in the reported $(A)[Mo_5O_{16}]$ materials obeys the same interacting scheme including a similar positioning of the ammonium heads of the A^{2+} cations toward the steps of the $^2/_\infty[Mo_nO_{3n+1}]^{2-}$ blocks, with the establishment of very similar hydrogen-bonding networks between both the organic and inorganic components. The observed systematic organization is consistent with our assumption that the increase of the POM dimensionality (from 0D clusters or 1D chains to 2D layers) allows better control of the organic–inorganic interface during the self-assembling processes. The overall size of the A^{2+} cations drastically influences the topology of the $^2/_\infty[Mo_nO_{3n+1}]^{2-}$ blocks in **1** and **2**, and the steric hindrance of the ammonium heads is a pertinent parameter to take into account. This opens up a way to the controlled fabrication of hybrid materials containing new $^2/_\infty[Mo_nO_{3n+1}]^{2-}$ layers with n higher than 9 in the future via the proper choice of A^{2+} cations having higher overall sizes. Moreover, the $^2/_\infty[Mo_nO_{3n+1}]^{2-}$ blocks (n = 5, 7, 9) are perfectly distinguishable by FT-Raman spectroscopy, and a good empirical correlation between the layer topologies and their Mo_2O stretching vibration frequencies has been established at a quantitative level. Finally, these $^2/_\infty[Mo_nO_{3n+1}]^{2-}$ layer-containing materials can be viewed as intermediate species between classical POM clusters or chains and α-MoO_3 slabs. Consequently, they deserve deep investigations on their chemical and physical properties, in particular in relation to their potential interest for catalysis, photocatalysis, and photochromism. Such studies are thus in progress.

■ ASSOCIATED CONTENT

Supporting Information

Organic–inorganic interfaces in the reported $(A)[Mo_5O_{16}]$ materials and tables of bond valence sums for **1** and **2** and of Mo_2O stretching vibration frequencies of many $^2/_\infty[Mo_nO_{3n+1}]^{2-}$-containing hybrid compounds. This material is available free of charge via the Internet at http://pubs.acs.org.

■ AUTHOR INFORMATION

Corresponding Author

*E-mail: remi.dessapt@cnrs-imn.fr. Tel: +33 2 40 37 39 53. Fax: +33 2 40 37 39 95.

■ REFERENCES

(1) (a) Long, D.-L.; Burkholder, E.; Cronin, L. *Chem. Soc. Rev.* **2007**, *36*, 105–121. (b) Dolbecq, A.; Dumas, E.; Mayer, C. R.; Mialane, P. *Chem. Rev.* **2010**, *110*, 6009–6048. (c) Kortz, U.; Müller, A.; Salgeren, J. V.; Schnack, J.; Dalal, N. S.; Dressel, M. *Coord. Chem. Rev.* **2009**, *253*, 2315–2327. (d) Peng, Z. *Angew. Chem., Int. Ed.* **2004**, *43*, 930–935.

(2) (a) Han, J. W.; Hill, C. L. *J. Am. Chem. Soc.* **2007**, *129*, 15094–15095. (b) Zeng, H.; Newkome, G. R.; Hill, C. L. *Angew. Chem., Int. Ed.* **2000**, *39*, 1772–1774. (c) Noro, S.-I.; Tsunashima, R.; Kamiya, Y.; Uemura, K.; Kita, H.; Cronin, L.; Akutagawa, T.; Nakamura, T. *Angew. Chem., Int. Ed.* **2009**, *48*, 8703–8706. (d) Vazylyev, M.; Sloboda-Rozner, D.; Haimov, A.; Maayan, G.; Neumann, R. *Top. Catal.* **2005**, *34*, 93–99.

(3) (a) Rhule, J. T.; Hill, C. L.; Judd, D. A.; Schinazi, R. F. *Chem. Rev.* **1998**, *98*, 327–357. (b) Yamase, T. *J. Mater. Chem.* **2005**, *15*, 4773–4782. (c) Yamase, T. *Mol. Eng.* **1993**, *3*, 241–262. (d) Asenknopf, B. *Front. Biosci.* **2005**, *10*, 275–287. (e) Compain, J.-D.; Mialane, P.; Marrot, J.; Secheresse, F.; Zhu, W.; Oldfield, E.; Dolbecq, A. *Chem.—Eur. J.* **2010**, *16*, 13741–13748.

(4) (a) Hiskia, A.; Mylonas, A.; Papaconstantinou, E. *Chem. Soc. Rev.* **2001**, *30*, 62–69. (b) Guo, Y.; Hu, C. *J. Mol. Catal. A: Chem.* **2007**, *262*, 136–148. (c) Yang, Y.; Guo, Y.; Hu, C.; Wang, Y.; Wang, E. *Appl. Catal., A* **2004**, *273*, 201–210. (d) Schaming, D.; Allain, C.; Farha, R.; Goldmann, M.; Lobstein, S.; Giraudeau, A.; Hasenknopf, B.; Ruhlmann, L. *Langmuir* **2010**, *26*, 5101–5109.

(5) (a) Sanchez, C.; Soler-Illia, G. J.; de, A. A.; Ribot, F.; Lalot, T.; Mayer, C. R.; Cabuil, V. *Chem. Mater.* **2001**, *13*, 3061–3083. (b) Muller, A.; Kogerler, P.; Kuhlmann, C. *Chem. Commun.* **1999**, *15*, 1347–1358. (c) Müller, A.; Kogerler, P.; Dress, A. W. M. *Coord. Chem. Rev.* **2001**, *222*, 193–218. (d) Long, D.-L.; Tsunashima, R.; Cronin, L. *Angew. Chem., Int. Ed.* **2010**, *49*, 1736–1758. (e) Kang, Z.; Wang, E.; Mao, B.; Su, Z.; Gao, L.; Lian, S.; Xu, L. *J. Am. Chem. Soc.* **2005**, *127*, 6534–6535.

(6) (a) Compain, J.-D.; Deniard, P.; Dessapt, R.; Dolbecq, A.; Oms, O.; Sécheresse, F.; Marrot, J.; Mialane, P. *Chem. Commun.* **2010**, *46*, 7733–7735. (b) Wang, Y.; Li, W.; Wu, L. *Langmuir* **2009**, *25*, 13194–13200. (c) Li, H.; Qi, W.; Li, W.; Sun, H.; Bu, W.; Wu, L. *Adv. Mater.* **2005**, *17*, 2688–2692. (d) Zhang, T.; Liu, S.; Kurth, D. G.; Faul, C. F. J. *Adv. Funct. Mater.* **2009**, *19*, 642–652.

(7) (a) Akutagawa, T.; Endo, D.; Noro, S.-I.; Cronin, L. *Coord. Chem. Rev.* **2007**, 2547–2561. (b) Yan, Y.; Wang, H.; Li, B.; Hou, G.; Yin, Z.; Wu, L.; Yam, V. W. W. *Angew. Chem., Int. Ed.* **2010**, *49*, 9233–9236. (c) Streb, C.; Long, D.-L.; Cronin, L. *CrystEngComm* **2006**, *8*, 629–634. (d) Reinoso, S.; Dickman, M. H.; Reicke, M.; Kortz, U. *Inorg. Chem.* **2006**, *45*, 9014–9019. (e) Li, H.; Sun, H.; Qi, W.; Xu, M.; Wu, L. *Angew. Chem., Int. Ed.* **2007**, *46*, 1300–1303.

(8) (a) Bar-Nahum, I.; Cohen, H.; Neumann, R. *Inorg. Chem.* **2003**, *42*, 3677–3684. (b) Bar-Nahum, I.; Narasimhulu, K. V.; Weiner, L.; Neumann, R. *Inorg. Chem.* **2005**, *44*, 4900–4902. (c) Mialane, P.; Zhang, G.; Mbomekalle, I. M.; Yu, P.; Compain, J.-D.; Dolbecq, A.; Marrot, J.; Secheresse, F.; Keita, B.; Nadjo, L. *Chem.—Eur. J.* **2010**, *16*, 5572–5576.

(9) (a) Yamase, T. *Chem. Rev.* **1998**, *98*, 307–325. (b) Dessapt, R.; Collet, M.; Coué, V.; Bujoli-Doeuff, M.; Jobic, S.; Lee, C.; Whangbo, M.-H. *Inorg. Chem.* **2009**, *48*, 574–580. (c) Coué, V.; Dessapt, R.; Bujoli-Doeuff, M.; Evain, M.; Jobic, S. *Inorg. Chem.* **2007**, *46*, 2824–2835. (d) He, T.; Yao, J. *Prog. Mater. Sci.* **2006**, *51*, 810–879.

(10) (a) Duraisamy, T.; Ramanan, A.; Vittal, J. J. *J. Mater. Chem.* **1999**, *9*, 763–767. (b) Coué, V.; Dessapt, R.; Bujoli-Doeuff, M.; Evain, M.; Jobic, S. *J. Solid State Chem.* **2006**, *179*, 3615–3627. (c) Hubbard, D. J.; Johnston, A. R.; Sanchez Casalongue, H.; Narducci Sarjeant, A.; Norquist, A. J. *Inorg. Chem.* **2008**, *47*, 8518–8525. (d) Chen, L.-J.; He,

X.; Xia, C.-K.; Zhang, Q.-Z.; Chen, J.-T.; Yang, W.-B.; Lu, C.-Z. *Cryst. Growth Des.* **2006**, *6*, 2076−2085. (e) Vitoria, P.; Ugalde, M.; Gutierrez-Zorrilla, J. M.; Roman, P.; Luque, A.; San Felices, L.; Garcia-Tojal, J. *New J. Chem.* **2003**, *27*, 399−408.
(11) (a) Evain, M.; Petricek, V.; Coué, V.; Dessapt, R.; Bujoli-Doeuff, M.; Jobic, S. *Acta Crystallogr.* **2006**, *B62*, 790−797. (b) Veltman, T. R.; Stover, A. K.; Narducci Sargeant, A.; Min Ok, K.; Shiv Halasyamani, P.; Norquist, A. J. *Inorg. Chem.* **2006**, *45*, 5529−5537. (c) Hagrman, D.; Warren, C. J.; Haushalter, R. C.; Seip, C.; O'Connor, C. J.; Rarig, R. S. Jr.; Johnson, K. M. III; LaDuca, R. L. Jr.; Zubieta, J. *Chem. Mater.* **1998**, *10*, 3294−3297.
(12) Dessapt, R.; Kervern, D.; Bujoli-Doeuff, M.; Deniard, P.; Evain, M.; Jobic, S. *Inorg. Chem.* **2010**, *49*, 11309−11316.
(13) Petricek, V.; Dusek, M.; Palatinus, L. *JANA2006, a Crystallographic Computing System*; Institute of Physics, Academy of Sciences of the Czech Republic: Prague, Czech Republic, 2000.
(14) Oszlányi, G.; Suto, A. *Acta Crystallogr., Sect. A: Found. Crystallogr.* **2004**, *60*, 134−141.
(15) Palatinus, L. *Acta Crystallogr., Sect. A: Found. Crystallogr.* **2004**, *60*, 604−610.
(16) Palatinus, L.; Chapuis, G. *J. Appl. Crystallogr.* **2007**, *40*, 786−790.
(17) Brandenburg, K. *Diamond*, version 3; Crystal Impact GbR: Bonn, Germany, 2001.
(18) (a) Nelson, J. H.; Johnston, A. R.; Narducci Sarjeant, A.; Norquist, A. *Solid State Sci.* **2007**, *9*, 472−484. (b) Sun, D.; Zhang, H.; Zhang, J.; Zheng, G.; Yu, J.; Gao, S. *J. Solid State Chem.* **2007**, *180*, 393−399.
(19) Xu, Y.; An, L.-H.; Koh, L.-L. *Chem. Mater.* **1996**, *8*, 814−818.
(20) (a) Guillou, N.; Ferey, G. *J. Solid State Chem.* **1999**, *147*, 240−246. (b) Yan, B.; Maggard, P. A. *Inorg. Chem.* **2006**, *45*, 4721−4727. (c) Coué, V.; Dessapt, R.; Bujoli-Doeuff, M.; Evain, M.; Jobic, S. *J. Solid State Chem.* **2008**, *181*, 1116−1122. (d) Wessels, A. L.; Jeitschko, W. *J. Solid State Chem.* **1997**, *128*, 205−208.
(21) (a) Gatehouse, B. M.; Miskin, B. K. *Acta Crystallogr.* **1975**, *B31*, 1293−1299. (b) Zavalij, P. Y.; Whittingham, M. S. *Acta Crystallogr.* **1997**, *C53*, 1374−1376. (c) Zapf, P. J.; Haushalter, R. C.; Zubieta, J. *Chem. Commun.* **1997**, *3*, 321−322.
(22) Andersson, G.; Magnéli, A. *Acta Chem. Scand.* **1950**, 793−797.
(23) Seguin, L.; Figlarz, M.; Cavagnat, R.; Lassegues, J.-C. *Spectrochim. Acta, Part A* **1995**, *51*, 1323−1344.